17
Hollows, colluvium, and landslides in soil-mantled landscapes

William E. Dietrich, Cathy J. Wilson, and Steven L. Reneau

Abstract

Field measurements from 23 sites in California and from five other widely distributed locations on soil-mantled hillslopes reveal a strong inverse relation between maximum drainage area of unchannelized basins and their average hollow gradients. The area–slope product was found to equal about 4000 m^2. Hollow length was also negatively correlated to average hollow gradient. These observations indicate that the number of sources and, consequently, drainage density increase with slope. The conservation of mass equation for a tipped triangular trough and a slope-dependent transport law are used to develop an expression for the rate of colluvium accumulation in hollows. Maximum colluvium depth is found to increase by the one-half power of time owing to the vertically increasing cross-sectional area of the trough. Rate of accumulation is proportional to side-slope gradient and to the difference between the side-slope and hollow gradient. The ratio of hollow to side-slope gradient is typically about 0.8. Models of shallow subsurface flow and deeper ground water flow are used to predict, via the Mohr–Coulomb failure criterion, the relation of hollow length to its gradient. It is not yet known which flow path plays the dominant role in controlling the position of the channel head, but both models predict that angle of internal friction ϕ' of the colluvium or weathered bedrock strongly influences the size and slope of the unchannelized basins and that basin size must rapidly decline above a gradient of 0.7 tan ϕ'.

Introduction

As a consequence of the seminal work by Hack and Goodlett (1960) and the numerous field studies that their study stimulated, it is now becoming widely recognized that small unchannelized valleys (Fig. 17.1) dominate the drainage

Figure 17.1 View of unchannelized basins on hillslopes in Marin County, California. Note tributaries or subhollows within larger unchannelized basins.

area of most soil-mantled hillslopes and greatly influence runoff and sediment transport processes. The valleys focus shallow subsurface storm flow or throughflow, which may produce high pore pressures and saturation overland flow, in the downslope ends of the valleys. The spoon-shaped surface topography also forces the convergence of soil material transported downslope by creep and biogenic transport processes, and consequently the valleys tend to develop a thick mantle of colluvium (e.g., Hack and Goodlett, 1960; Pierson, 1977; Dietrich and Dunne, 1978; Marron, 1982; Lehre, 1982; Woodruff, 1971; Reneau et al., 1984). Landslides most commonly occur in these topographic convergent zones (e.g. Pierson, 1977; Tsukamoto et al., 1982; Shimokawa, 1984; Dietrich and Dunne, 1978; Woodruff, 1971; Hack and Goodlett, 1960; Lehre, 1982; Iida and Okunishi, 1983) and the thick deposits tend to produce large rapid debris flows that scour to bedrock the first- and second-order channels that lie downslope (Pierson, 1977; Dietrich and Dunne, 1978; Swanston and Swanson, 1976). Debris flows from thick colluvium in unchannelized valleys have caused considerable destruction of property and loss of life (Brown, 1984; Reneau et al., 1984; Woodruff, 1971; Tsukamoto et al., 1982) and play a major role as sediment sources in catchment-level sediment budgets (Dietrich and Dunne, 1978; Lehre, 1982; Swanson et al., 1982; Pierson, 1977).

A qualitative model is fairly well established for how the unchannelized valleys work. In essence, the valleys are sites that experience infrequent, but recurrent rapid evacuation of colluvium, primarily by landsliding, followed by periods of slow colluvium accumulation (Hack and Goodlett, 1960; Woodruff, 1971; Pierson, 1977; Calver, 1978; Dietrich and Dunne, 1978; Kirkby, 1978; Humphrey, 1982; Lehre, 1982; Shimokawa, 1984). The convergent subsurface flow in the spoon-shaped bedrock geometry leads to highest pore pressures in the lower portion of the valley. These pore pressures may be further enhanced by the discharge of deeper ground water in the hollow. Under a certain combination of colluvium strength and antecedent moisture conditions, storm precipitation can produce failure in the colluvium. Weathering and soil development may produce permeability and strength boundaries such that failures occur within the colluvium (Reneau et al., 1984; Tsukamoto and Kusakobe, 1984). The landslide may only partially evacuate the colluvial mantle, after which sheetwash and gullying may continue to erode the exposed slide scar. In some cases, gullying may be the primary cause of colluvium removal. Revegetation on the scar contributes significantly to reestablishing accumulation in the hollow (Lehre, 1982; Shimokawa, 1984).

The frequency of flushing events in hollows is not yet well documented. Shimokawa (1984) used dendrochronology and soil thickness measurements on landslide scars of various ages in steep, forested hillslopes of Japan to estimate recurrence interval of landsliding in hollows and adjacent slopes. As Iida and Okunishi (1983) have also proposed, Shimokawa suggested that recurrence of landsliding is largely controlled by the rate of "top-soil" accumulation because landsliding is thought to be very likely once the soil

reaches a critical depth. Estimated recurrence for landslides at a site varied with bedrock type and slope gradient from 12 to 30 years on 50–70° slopes developed on ash and pumice to about 1000 years on 20–40° slopes developed on granite. In the Pacific Northwest of the U.S.A., dendrochronology has been useful in giving estimates of the rate of deposition in hollows in the early phase of post-landslide accumulation (Dietrich and Dunne, 1978), but it appears that for the vast majority of sites the recurrence of major flushing is much greater than can be ascertained from this method. Palynology (Dietrich and Dorn, 1984) and radiocarbon dating of thick colluvial deposits in hollows in the California Coast Ranges and Tehachapi Mountains (Marron, 1982; Reneau et al., 1984 and in preparation) suggest that the frequency of erosion of colluvium to the bedrock surface is of the order of 10 000 years. Six of nine sites dated, however, yield basal ages between 11 000 and 14 500 B.P. (Reneau et al., in preparation), and it may be that these hollows record a period of more frequent, intense storms. Much work is still needed to sort out the significance of climatic fluctuations. We see both landsliding and net accumulation under current climatic conditions, hence climatic change is not required to induce either net accumulation or erosion in individual hollows. A similar conclusion was reached by Hack and Goodlett (1960) for hollows in the Appalachian Mountains, and by Gray and Gardner (1977) for colluvial deposits on hillslopes of the Appalachian Plateau.

There is now a need to develop quantitative, physically based models for the hydrology, sediment transport, weathering, and instability of the colluvium and link these models to predict the geometry of unchannelized basins. Some valuable first steps have been taken in modeling subsurface flow in small unchannelized bedrock valleys using finite-element methods (Humphrey, 1982) and contributing-area concepts (Humphrey, 1982; Iida, 1984; Kirkby, 1978). Iida and Okunishi (1983) treated the stability problem as being entirely dependent on the depth of colluvium, and modeled the lowering rate of the bedrock surface as a function of the rate of colluvium accumulation and bedrock weathering, which in turn control the recurrence interval of landsliding.

In this chapter, we focus on the end-member problem of what controls the size and shape of the largest unchannelized basins on hillslopes—that is, those basins large enough to support channelized flow at their downslope ends. In essence we ask: How much drainage area in a basin does it take to initiate a channel? We first present field data on area, length, and slope relationships of such basins and then analyze the shape of the basins and the accumulation of colluvium in the hollow. Finally, through the use of simple flow models and slope stability calculations we propose a quantitative explanation for the observed field relationships.

Basin geometry

Other than the qualitative impression that the colluvium-mantled bedrock

valleys appear to be typically spoon-shaped with concave contours and concave-up downslope axes, little is known about the geometry of these features. To describe the large-scale, three-dimensional properties of slopes, Hack and Goodlett (1960) introduced the now widely used terminology of *nose* for convex contours, *side slope* for straight contours, and *hollow* for concave contours. Typically all three elements make up the basin upslope of the head of the channel. Marcus (1980) proposed a morphologic classification of first-order basins based in part on the planform shape of the unchannelized valley in the first-order basins. Tsukamoto et al. (1982) computed the areal proportions of convergent, divergent, or planar slopes in Japanese catchments. On average, convergent slopes make up 60 percent of the entire basin area. Tsukamoto et al. propose calling convergent slope areas zero-order basins and state that these are sites of ephemeral streams during heavy storms.

Four measures of unchannelized basin geometry that are fairly simple to obtain and appear to be quite useful are (1) the drainage area of the basin upslope of the channelway, (2) the maximum horizontal length of the axis of the basin, (3) the hollow and side-slope gradients, and (4) the basin amplitude (Fig. 17.2). The first three measures involve careful field inspection to locate the farthest downslope extent of the unchannelized, colluvial portion of the hollow (axial region of the basin). The average hollow gradient, which will be used in the analysis to follow, is computed as the elevation difference between ridge crest and channel head divided by the horizontal distance. In general, the hollows that are direct upslope extensions of the first-order channels rather than tributaries to them will be the largest unchannelized basins. After

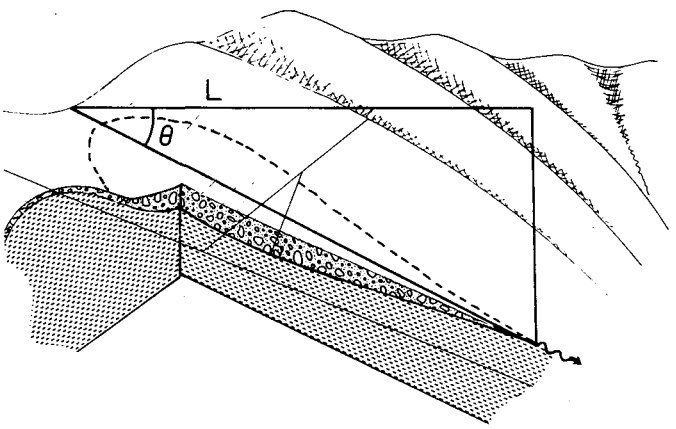

Figure 17.2 Illustration of the geometric properties of unchannelized basins. L and θ are the horizontal length and average gradient of the hollow, respectively. Basin amplitude is the distance from the bedrock to the horizontal line between the noses along a line normal to the bedrock surface in the hollow axis. The broken line encloses the depositional zone in the hollow.

erosional events, the channel head may temporarily extend well up the hollow, as described by Hack and Goodlett (1960) and many other subsequent authors; hence for the purpose of defining the maximum unchannelized basin geometry, the hollows without significant evidence of recent flushing should be used. Alternatively, basins can be randomly sampled without regard to recent flushing and trends in geometry can be established using the largest unchannelized basins encountered. The fourth measure, basin amplitude, quantifies how deeply the hollow is incised relative to adjacent interfluves. Amplitude can be computed from a detailed topographic map and information on thickness of the colluvium in the hollow. A straight line can be drawn across the basin connecting points of equal elevation on adjacent drainage divides on the noses. The maximum difference in elevation along this line between the nose and the bedrock surface of the hollow multiplied by the cosine of the interfluve slope is a measure of basin amplitude. The thickness of the colluvium in the hollow can be determined by drilling, by examining exposure in landslide scars, by using geophysical methods, such as seismic refraction, or by employing some combination of these techniques. As amplitude will vary along the basin, for purposes of comparison, maximum amplitude is used.

Observations

Results of field surveys in northern California and comparison with sites elsewhere raise several intriguing questions regarding basin geometry and controls on channel inception. Basins in the rounded, soil-mantled hillslopes just north of San Francisco in Marin County were selected to obtain a broad range in hollow gradient. Sites are underlain by chert, greenstone, and sandstone of the Franciscan assemblage and have a cover of dense grass, coastal scrub vegetation or mixed hardwood (oak, laurel, madrone) forest. Mean annual precipitation is about 600–900 mm. Debris flows from colluvium-mantled hollows are common in this area, and many sites could not be used because of recent landsliding. Basins were selected to sample the range of hollow gradients, and surveying was accomplished either with a hand-level and tape or with a theodolite. Often 1 : 24 000-scale topographic maps were used to define drainage area.

Slope profiles of the ground surface of hollows in Marin County and at other locations show considerable variation. Except for a short convex ridge, many are nearly straight or concave throughout, whereas others only become either noticeably convex or concave as the channel head is approached. Often there is an abrupt change in slope from the hollow to the channelway, and it is likely that near the channel head a large increase in bedrock slope leads to a convex profile in the colluvial fill, whereas a strong decrease in bedrock slope results in a concave colluvial slope profile. A large change in slope from hollow to channelway probably significantly affects the groundwater flow and consequent pore pressures develop in the downstream end of the colluvial deposit. For three cases where a strong steepening of slope was observed, the

hollow and local channelway slopes were averaged and data were noted separately (Fig. 17.3). It is not yet clear whether this averaging procedure is the best representation of field relationships. In two gentle profiles with gradients less than 10°, discontinuous gullies were present 50–70 m upslope from the continuous channel head, and in one case, winter storm flow discharged from a large pipe in the upper part of the discontinuous gully. Regardless of surface slope, the longitudinal profile of the underlying bedrock surface in hollows appears generally to be concave-up (Reneau et al., 1984; Dietrich and Dorn, 1984; Pierson, 1977; Iida and Okunishi, 1983).

Drainage area of surveyed unchannelized basins in Marin County increases in proportion to the 1.2 power of the total hollow length (Fig. 17.3A). This low rate of increase in area with hollow length implies that small and large basins differ more in their length than in their width. As Hack and Goodlet (1960) originally noted, however, area increases quite rapidly with distance down the hollow within individual basins.

Data from field sites in Marin County reveal an inverse relationship between drainage area upslope of the channel head and average hollow gradient (Fig. 17.3B). The most accurate field data give area proportional to the -1.04 power of hollow gradient. Area is proportional to the -0.99 power of hollow

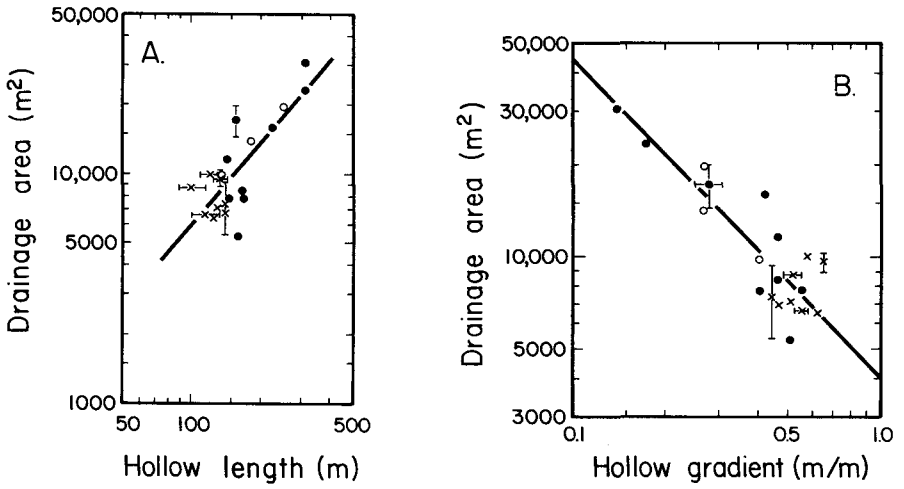

Figure 17.3 Drainage area upslope of channel head in small catchments as a function of (A) horizontal length of hollow and (B) hollow gradient for hillslopes in Marin County, immediately north of San Francisco, California. Open circles represent sites in which slope strongly steepened downstream of the channel head and the average of upslope and downslope gradients on either side of the channel head was used (unpublished data from K. Whipple and P. Templet, University of California, Berkeley, 1984). The crosses represent forested sites where landslide scars are common and make it more difficult to define precisely the channel head. Error bars denote range of uncertainty. The full line in (A) represents the least-squares regression equation $A = 22.9\,L^{1.21}$, $r = 0.79$, $n = 20$.

gradient for the entire 20-point data set. Hence the area–slope product is essentially a constant and for the nine data points represented by full circles in Figure 17.3B the constant is 4043 m^2. If all available data for Marin County are used in conjunction with eight other data points from gravelly soils in northern California, Oregon, Virginia, and Japan to define the area–slope correlation, essentially the same result is obtained (Fig. 17.4). In this case, area decreases in proportion to the -1.05 power of hollow gradient and the area–slope product equals 4121 m^2. There are, of course, many smaller unchannelized basins that intersect as tributaries to channels or other hollows (Fig. 17.1) before they capture sufficient drainage area to produce a channel. Strong geologic controls may force ground water toward the surface, which can generate sufficient pore pressure and consequent instability to initiate and maintain a channel in basins smaller or less steep than expected from Figure 17.4. With more data, it may be possible to detect differences due to geology, climate, or vegetation. This small sample suggests, however, that in general the area–slope product necessary to maintain a channel head at the end of an unchannelized basin in well-vegetated, coarse-textured colluvium on a soil-mantled hillslope is a constant and equals about 4000 m^2.

Data from the sites used in Figure 17.4 also show a strong decrease in total hollow length with increasing gradient (Fig. 17.5). For all 28 data points, length decreased proportionally to the -0.67 power of slope. For example, a

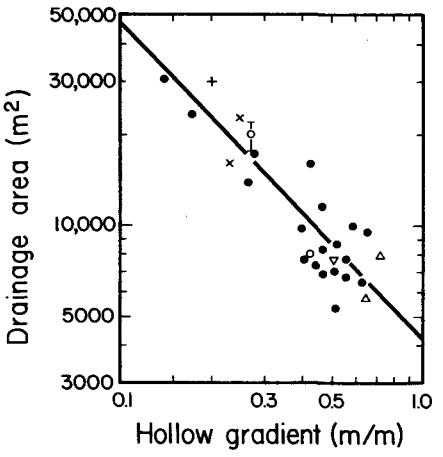

Figure 17.4 Relationship between drainage area and hollow gradient for basins upslope of channel heads in Marin County, California (●), Clear Lake, California (+ , Dietrich and Dorn, 1984), coastal northern California (× , W. Trush, University of California, Berkeley, unpublished data, 1984), Virginia (○, without bar, Hack and Goodlett, 1960; ○, with bar, W. Dietrich, unpublished data, 1984), Japan (▽ , Tanaka, 1982), and central coastal Oregon (△ , Pierson, 1977, personal communication, 1984). The full line represents the regression equation $A = S^{-1.05}$, $r = -0.885$, $n = 28$.

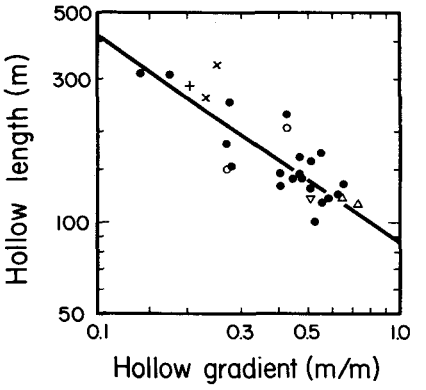

Figure 17.5 Relationship of hollow length to average gradient for unchannelized basins. Symbols are the same as in Figure 17.4. The regression equation is $L = 87.7S^{-0.67}$, $r = -0.823$, $n = 28$.

hollow with a 10° slope should be about 281 m long, whereas a steeper, 30° hollow should be only about 127 m long. Because the hollow gradient equals the total elevation drop from ridge to channel head divided by horizontal length of the basin, the regression equation indicates that hollow length decreases as the -2.0 power of elevation drop.

The length–slope observation has important implications for drainage density. The area required to initiate a channel head is also the area necessary to produce a source for an exterior link. Hence, the maximum number of sources in a basin equals the basin drainage area divided by the observed area required to initiate a channel. Clearly, the actual number of sources will be much less because most of a drainage basin drains to the sides rather than to the heads of channels. Nonetheless, the inverse relationship between area and slope shown in Fig. 17.4 would suggest that the number of sources in a basin is directly correlated with slope. Intuitively, one would expect that the greater the number of sources in a drainage basin, the greater the drainage density. This intuition is confirmed if certain simple assumptions are made (R. Shreve, personal communication, 1985). If we assume that in a large drainage basin the number of exterior links, which is the same as the number of sources, is equal to the number of interior links, and we denote the number of sources *per unit area* by N, then the drainage density D is

$$D = \frac{2N\bar{l}_L}{2N\bar{a}_L} \tag{1}$$

for a given mean link length $\bar{l}_L$ and link area $\bar{a}_L$. Because $\bar{a}_L = 1/(2N)$ and $\bar{l}_L^2 = K\bar{a}_L$ (see discussion in Abrahams (1984)), where K is a constant, the drainage density can also be expressed as

$$D = (2KN)^{0.5} \tag{2}$$

Thus our empirical area–slope relationship implies that steeper basins of a given drainage area with more sources, have higher drainage density than gentler basins of the same area with fewer sources. These preliminary data support the inference by Dunne (1980) that in regions where subsurface flow, and consequent piping and landsliding, play a major role in landscape evolution, drainage density is higher on steeper slopes.

Limited data (four sites) from northern California on basin amplitude suggest that the amplitude divided by the half-width of the basins is roughly equal to the hollow gradient. For example, a 100-m wide basin on a 9° slope would have 8 m elevation difference between the interfluve and the hollow, whereas a 60-m wide basin on a 27° slope would have 15 m elevation difference. Although unchannelized basins tend to be narrower on steeper slopes, the steeper gradient of the hollow results in greater hollow amplitude.

Because the gradients down the interfluves, down the hollow, and from the interfluve to the hollow are similar, it is reasonable to suggest that the gradients are controlled by the same mass-wasting processes. We cannot as yet predict these gradients.

Sediment transport

On well-vegetated, soil-mantled hillslopes, soil is transferred downslope by the mass movement processes of landslides, creep, and biogenic transport. Landsliding is rare on noses or side slopes to hollows. On hillslopes where soil properties and biologic activity are relatively uniform, rates of creep and biogenic transport are probably primarily dependent on slope gradient. Hence, in unchannelized basins, the focusing of colluvium toward the hollow, which is generally less steep than the side slopes, results in net deposition and a thickening of colluvium over time.

Landslide processes involving the colluvial deposits in the hollow appear to vary with texture. Instability in clay-rich colluvium tends to produce slow-moving earthflows (e.g., Keefer and Johnson, 1984): in a single season total displacement of the center of mass of the colluvial fill may be only a few meters or tens of meters. Movement is periodic and the intervals of inactivity can be sufficiently long that the landslide morphology (such as the crown scarp and the lobate snout) may be indistinct. In contrast, landslides in coarse-textured colluvium in hollows, which are the focus of this paper, typically initiate as a slide but quickly liquefy, producing a rapidly flowing debris flow (e.g., Pierson, 1977). Liquefaction of colluvium may be caused by the sudden slide-induced increased shear that affects an undrained loading condition. Recent work by Kramer (1985) has demonstrated that loose fine sand will liquefy when subjected to undrained shear, and he has suggested that coarser debris will act similarly. Typically only a portion of the accumulated colluvium in the hollow is discharged with the debris flow. Subsequent gullying and slumping may

erode a large portion of the remaining colluvium before net accumulation is initiated.

In the following discussion, we examine two simple models for colluvium accumulation in hollows. There are several reasons to build such models. At least in the early phases of deposition in a hollow after a flushing event, increasing colluvium thickness should lead to less stable deposits because of the progressively reduced effectiveness of the apparent cohesion provided by roots (Dietrich and Dunne, 1978). Hence, an important linkage may exist between rate of infilling and frequency of instability (see also Pierson, 1977, p. 133). As mentioned above, Iida and Okunishi (1983) proposed a deterministic model that predicts failure of colluvium once it reaches a critical thickness. The colluvium was assumed to be saturated, and they stated that intense saturation-producing storms in Japan are sufficiently frequent for this to be a reasonable assumption. On the steep slopes of the coastal mountains in the western United States, however, colluvium in many areas has reached thicknesses much greater than that which can be easily saturated, perhaps due to an extended period in the Holocene with a low frequency of intense rainstorms (Reneau et al., in preparation). Colluvium thickness in hollows ranges from less than 1 m to over 10 m, but typical maximum depth is 4–5 m (Reneau et al., 1984). If rates of deposition can be predicted, some of the observed variations may be explicable quantitatively in terms of basin geometry and time since flushing. Finally, develoment of a sediment transport model will provide some insight into the form of the transport law (*sensu* Kirkby, 1971; Smith and Bretheron, 1972) controlling soil transport and the morphology of the nose and side slopes contributing to the hollow accumulation. This sediment transport model should allow us to explore the adjustments in slope, soil thickness, and transport rates for different bedrock.

A conical basin

The most convenient mathematical representation of an unchannelized basin is that of a slice of a cone (Fig. 17.6). As Carson and Kirkby (1972, p. 392) have shown, the mass balance equation for colluvium transport in a cylindrical

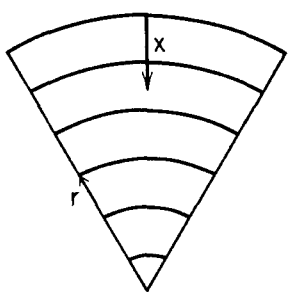

Figure 17.6 Coordinate system for conical-shaped basins.

coordinate system (Fig. 17.6) in which the mass transport law is

$$q_s = -a\frac{\partial z}{\partial x} \tag{3}$$

can be written as

$$-a\frac{\partial^2 z}{\partial x^2} - \frac{a}{r}\frac{\partial z}{\partial x} = -\frac{\partial z}{\partial t} \tag{4}$$

The first term in (4) is the diffusion component in which a is the transport coefficient, z is the elevation above an arbitrary datum, and x is the distance downslope from the ridge crest (Fig. 17.6). The second term arises from the convergence caused by contour concavity and increases as the distance from the basin outlet r decreases. The last term is the local elevation change of the colluvial surface with respect to time t. Equation (4) can be solved numerically for a variety of upslope and downslope boundary conditions. If profile concavity is small then the diffusion component is negligible and (4) yields

$$h \approx \frac{a}{r} St \tag{5}$$

where h is the thickness of the accumulated colluvium and S is the constant slope. Depth of colluvium increases downslope linearly with time. For a given amount of time since onset of deposition, thickness is proportional to slope. More complex results, involving significant contribution from the diffusion component, can be obtained if profile concavity is allowed and the effects of discharge at the end of the basin are permitted to propagate upslope and alter the surface slope. This seems unwarranted, however, because the basin geometry, although mathematically convenient, does not appear to represent natural basins.

Inspection of unchannelized basins in the field or on sufficiently detailed topographic maps (1- to 2-m contour interval) confirms Hack and Goodlett's (1960) observation that such basins are best described as having convex contours (nose) along a narrow drainage divide and straight contours (side slopes) between the nose and the hollow. The side-slope element, which is the transportation surface of colluvium to the hollow, is not well represented by the coordinate system shown in Figure 17.6 and used in (4) and (5). This geometry also does not yield the pronounced 'U' or 'V' shaped cross-sections typically revealed in road-cut exposures across hollows. Finally, unchannelized basins, although spoon-shaped, tend to be long relative to their widths and to have subparallel rather than strongly convergent interfluves.

A trough-shaped basin

We propose that a more realistic representation of an unchannelized basin is that of a tipped triangular trough. As illustrated in Figure 17.7A, sediment

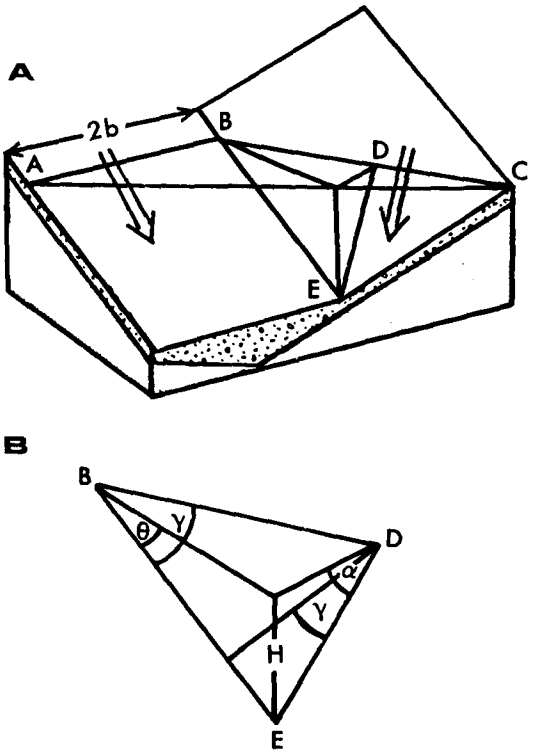

Figure 17.7 (A) Diagram of an unchannelized basin represented as a tipped triangular trough. The horizontal plane ABC intersects the surfaces of the colluvium-mantled hollow and side slopes along contours AB and BC, respectively. Note that convergent transport, represented by arrows, leads to accumulation of thick deposits of colluvium. (B) Geometric relationships of hollow gradient θ side-slope gradient α and the angle γ formed between a line parallel to the side slope and perpendicular to the depositional zone in the hollow.

transport from straight contour side slopes intersects the less steep hollow at an acute angle. The trough is composed of a source area of side slopes, where the soils are thin, and a depositional zone of thicker colluvium in the hollow. With increasing depth of colluvium, the cross-sectional area increases rapidly and produces a distinct 'V' shaped deposit. Profile concavity of the trough axis is not considered in this geometric model, although the model can be modified to include this feature. The nose is reduced to a line, but this should have negligible effect on deposition of colluvium in the hollow. Perhaps more importantly, creep and biogenic transport processes will tend to make the slope transition from the side slope to the hollow less abrupt, probably leading to straight contours on accumulated colluvium along the hollow boundary. This effect will not be considered here, as it is viewed as nonessential to understanding the form of deposition over time.

To model the deposition of colluvium in the tipped trough we make several simplifying assumptions. (1) Typically the upslope ends of unchannelized basins are curved, and a more complete representation of the basin would be to include at the upslope end of the trough a short conical form similar to that depicted in Figure 17.6. We assume here that contribution of colluvium to the upslope end of the trough from the curved end is exactly balanced by the colluvium discharged at the downslope end of the basin. This implies that although some side-slope colluvium is discharged out of the basin, it is replaced with that from the upslope end of the basin. In this case, then, the change in volume with time of colluvium in the hollow equals the discharge of colluvium from the side slopes into the depositional zone. (2) As the deposit thickens in the hollow, the slope of the colluvial fill remains constant. (3) The downslope transport rate on the side slope q_S is expressed by equation (3), rewritten here as

$$q_S = a \tan \alpha \tag{6}$$

where α is the angle of the side slope (Fig. 17.7B).

Sediment from the side slope enters the depositional zone at an angle (Fig. 17.7A). Inspection of Figure 17.7B reveals that the component of transport normal to the depositional zone q_{Sn}, is

$$q_{Sn} = q_S \cos \gamma \tag{7}$$

where γ is the angle between the transport direction perpendicular to the side slope contours and the transport perpendicular to the depositional zone, which is assumed to lie parallel to the axis of the trough. Analysis of Figure 17.7B indicates that

$$\sin \gamma = (H/\sin \alpha)(H/\sin \theta)^{-1} \tag{8}$$

where H is the vertical height shown in Figure 17.7B and α and θ are the slopes of the side slope and hollow, respectively. Substitution of (8) and (6) into (7) yields

$$q_{Sn} = a \tan \alpha \left(1 - \frac{\sin^2 \theta}{\sin^2 \alpha}\right)^{1/2} \tag{9}$$

which can be simplifed to

$$q_{Sn} = a \left[\frac{\cos^2 \theta}{\cos^2 \alpha} - 1\right]^{1/2} \tag{10}$$

The total transport Q_{Sn} into the hollow of length l is then

$$Q_{Sn} = a2l \left[\frac{\cos^2 \theta}{\cos^2 \alpha} - 1\right]^{1/2} \tag{11}$$

Note than when the trough is horizontal, $\theta = 0$ and $Q_{Sn} = 2al \tan \alpha$, as required by the geometry of the basin. The conservation of mass equation for a depositional fill of volume V is

$$Q_{Sn} = \frac{dV}{dt} \tag{12}$$

The volume of the deposit at any time t is simply the cross-sectional area A times the length l of the deposit. The cross-sectional area is the half-width b times the maximum depth h of the fill measured perpendicularly to the bedrock axis in the hollow

$$A = bh \tag{13}$$

Again, analysis of the geometric relationships expressed in Figure 17.7B yields the following

$$b = h[\cos \theta \, (\tan^2 \alpha - \tan^2 \theta)^{1/2}]^{-1} \tag{14}$$

where h is measured perpendicular to the bedrock axis of the hollow, which is inclined at slope θ. Combining (13) and (14) gives the equation for the volume of the fill with the width term eliminated

$$V = h^2[\cos \theta \, (\tan^2 \alpha - \tan^2 \theta)^{1/2}]^{-1} l \tag{15}$$

The mass balance equation (12) can now be written using (11) and (15) as

$$a2l\left[\frac{\cos^2 \theta}{\cos^2 \alpha} - 1\right]^{1/2} = \frac{d}{dt}\,[h^2 (\cos \theta \, (\tan^2 \alpha - \tan^2 \theta)^{1/2})^{-1} l] \tag{16}$$

which gives

$$a \cos \theta \, (\tan^2 \alpha - \tan^2 \theta)^{1/2} \left[\frac{\cos^2 \theta}{\cos^2 \alpha} - 1\right]^{1/2} dt = h \, dh$$

Performing the integration and using the boundary conditions that $h = 0$ at $t = 0$ leads to

$$h = \left[a2 \cos \theta \, (\tan^2 \alpha - \tan^2 \theta)^{1/2} \left[\frac{\cos^2 \theta}{\cos^2 \alpha} - 1\right]^{1/2} t\right]^{1/2} \tag{17}$$

Inspection of available detailed topographic maps, including those reported by Hack (1965), indicates that the ratio of $\tan \theta$ to $\tan \alpha$ is typically about 0.8. This ratio probably ranges from 0.5 to 1.0. Substitution of possible slope combinations in $[(\cos^2 \theta / \cos^2 \alpha) - 1]^{1/4}$ shows that this term differs by less

than 20 percent from $(\tan^2 \alpha - \tan^2 \theta)^{1/4}$; hence, for simplicity, (17) can be reduced to

$$h = [a2 \cos \theta (\tan^2 \alpha - \tan^2 \theta)t]^{1/2} \tag{18}$$

and for $S_S = \tan \alpha$ and $S_h = \tan \theta$, it becomes

$$h = [a2 \cos \theta (S_S^2 - S_h^2)t]^{1/2} \tag{19}$$

Equation (19) shows that the depth increases in proportion to the 0.5 power of time after the onset of net deposition; hence the rate of increase in depth diminishes with time. This results from the increasing cross-sectional width with increasing depth in the triangular trough. In Figure 17.8, (19) is plotted for two ratios of hollow to side-slope gradient. For a given ratio, the maximum depth of colluvium at a given time is greater for steeper side slopes. Equation (19) also shows that the gradient difference between the hollow and side slope strongly influences accumulation rates. For example, the change in S_h/S_S from 0.8 to 0.5 depicted in Figure 17.8 results in a 45 percent increase in depth of colluvium.

For a given site, if the time since net deposition began can be determined then the coefficient a in the transport equation can be evaluated. Equation (19) can then be used to define quantitatively the thickness variations of colluvium with respect to time and slope. Reneau et al. (1984) report a radiocarbon date of 12 900 B.P. from charcoal in basal colluvium in a small, grass-covered basin with a maximum thickness of approximately 450 cm. From a detailed topographic map, the gradients of the hollow and side slope (which includes the edge of the depositional zone) were found to be 17° and 21°, respectively. Hence the ratio of the tangents of these two gradients is about 0.8. Equation

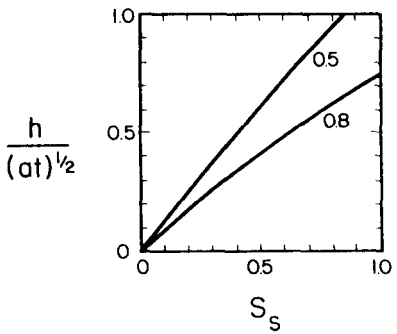

Figure 17.8 Relationship of the dimensionless ratio soil thickness h divided by the square root of the product of transport coefficient a and time t to side-slope gradient S_S for two different ratios (0.5 and 0.8) of hollow to side-slope gradients in a tipped triangular trough.

(19) can be rewritten to solve for a and, using the above values, yields $a = 152$ cm^3/cm yr. This value is relatively large as it is equivalent to the entire 30 cm thick soil column on the side slope moving downslope at the speed of 5 cm/yr. Biogenic transport caused by burrowing animals is quite apparent on the grass-covered hillslopes, but is probably not strong enough to cause this high transport rate (see discussion in Lehre (1982)). We have used a maximum value of colluvium depth rather than an average colluvium depth in the hollow axis of 400 cm, but this is a small correction. A large possible source of error in evaluating a is the assumption that the hollow was free of colluvium at 12 900 B.P. Reworking of colluvium not removed by a major erosional event should increase the apparent accumulation rates.

The simple sediment transport model based on the tipped triangular trough provides a quantitative tool for understanding the accumulation of colluvium in hollows. Extensive radiocarbon dating through vertical sections in hollows will allow direct testing of the form of the transport equation and evaluation of the transport coefficient. Such dates for different basins will also allow us to test the findings that the basin geometry strongly influences deposition rates in the hollow. Our first crude test points to a need to examine carefully the exposures of colluvium in hollows in order to identify stratigraphic or pedologic evidence for partial evacuation of colluvium and subsequent reworking. It also demonstrates the need for direct measurement of colluvium transport rates on side slopes.

Runoff and slope stability

The slope length or catchment area required to initiate a channel head must be one that provides sufficiently frequent runoff and high pore pressures that colluvium cannot accumulate further downslope. The instability that leads to flushing of colluvium in the hollow and temporary extension of the channel head upslope is not necessarily the same as that required to maintain the channel head in its farthest downslope position. Flushing of the colluvium is infrequent, occurring at intervals of hundreds to thousands of years, whereas the channelway appears to be the site where channelized flow and at least some alluvial transport regularly occur. The transition from the hollow to the channelway varies between basins. In some cases the channel gradually develops over a 5–10 m length of valley floor, but more often the channel head is an abrupt, steep wall in colluvium more than a meter in height. In this latter case we have seen abundant subsurface flow issuing from the base of the wall.

The specific mechanisms of channel-head maintenance are not yet well understood. In the California basins, the bed of the channel just downslope from the hollow is usually bedrock. Hence the channel is a seepage face draining the groundwater from the upslope unchannelized basin. As Dunne (1980) described, high seepage forces due to excessive pore pressures generated in the bedrock or colluvium may develop at channel heads and erode the

colluvium. On very steep basins, partial or complete saturation of the colluvium without excessive pore pressures, can be sufficient to cause landslides. This can occur frequently enough to maintain a channel head (Humphrey, 1982). Because of the dense vegetation cover in the downslope ends of hollows it seems unlikely that saturation overland flow could provide sufficient boundary shear stress to initiate a channel. Transport by the channelized flow at the channel head, however, should play some role in channelway maintenance, particularly in fine-grained colluvium where shallow flow is capable of significant transport. The distance downslope to the channel head also should be influenced by climate and thus vary with climatic change, although it is not obvious what precipitation characteristic should be most important.

In the following, we hypothesize that slope stability controls the location of the channel head and thereby directly or indirectly controls the size and geometry of the upslope unchannelized basin. We examine how shallow subsurface flow in the colluvial mantle, and excessive pore pressures generated from groundwater flow in the bedrock, may be responsible for the empirical relationships presented in the first part of this chapter. Throughout the following analysis we make the reasonable initial assumption that hollows have straight longitudinal profiles.

Shallow subsurface flow

If we represent the stability conditions leading to formation of a channel head with the infinite slope model of the Mohr–Coulomb failure law (e.g., Carson and Kirkby, 1972, p. 152), we can write for failure of colluvium of thickness z on a bedrock surface inclined at slope θ

$$\rho_s g z \sin\theta \cos\theta = c' + (\rho_s g z \cos^2\theta - \rho_w g h \cos^2\theta)\tan\phi' \qquad (20)$$

where ρ_s and ρ_w are the bulk density of colluvium and water, respectively, g is the gravitational acceleration, c' is the effective cohesion, ϕ' is the angle of internal friction, and h is the vertical height of saturated soil above the failure plane. If we can compute the saturation height h as a function of contributing area properties, then substitution into (20) will permit calculation of the length or area and hollow gradient that provide the saturation height requisite for slope failure.

Independently, Humphrey (1982) and Iida (1984) developed simple, analytic expressions for the depth of saturation caused by shallow subsurface flow during a specified rainstorm of constant intensity R_0 on a hillslope of simple geometry with isotropic hydraulic conductivity in the colluvium and an underlying impermeable bedrock. Under these conditions, the discharge at time t of subsurface flow per unit contour length $Q(t)$ is equal to the rainfall rate R_0 times the contributing area $a(t)$ per unit contour length at time t:

$$Q(t) = R_0 a(t) \qquad (21)$$

This is equivalent to Iida's equation (8) and Humphrey's equation (3.39). The discharge rate can be related to slope and soil properties via Darcy's law. The specific flux q for flow parallel to a bedrock boundary inclined with slope θ is

$$q = K_s \sin \theta \tag{22}$$

where K_s is the saturated hydraulic conductivity. The horizontal velocity component V_s is equal to $q \cos \theta$; thus

$$V_s = K_s \sin \theta \cos \theta \tag{23}$$

The discharge per unit contour length for a depth of saturation $h(t)$ becomes

$$Q(t) = h(t) K_s \sin \theta \cos \theta \tag{24}$$

Combining (24) and (21) and solving for $h(t)$ gives

$$h(t) = \frac{R_0\, a(t)}{K_s \sin \theta \cos \theta} \tag{25}$$

which is equivalent to Iida's equation (9) and Humphrey's equation (3.41). The maximum depth of saturation will be achieved when all of the catchment upslope of the channel head is contributing. Assuming uniform width, hence no flow convergence, (25) reduces to

$$h = \frac{R_0 L}{K_s \sin \theta \cos \theta} \tag{26}$$

The effect of flow convergence is treated somewhat differently by Iida and Humphrey, but both made use of a cylindrical coordinate system. Our previous analysis argues against this approximation and instead suggests that unchannelized basins are well represented by a tipped triangular trough. In this case the simplest approximation is to assume that shallow subsurface flow leaves the basin through the colluvium in the hollow; hence the ratio c of basin width to hollow width ($2b$) is a measure of the increased catchment area per unit contour length. Basin width is usually much larger than hollow width. As Hack (1965) pointed out, the basin to hollow width ratio may vary with hollow slope. Thus in (25) $a(t)$ equals cL (where L is basin length) for maximum saturation depth, which suggests that the consequence of flow convergence in a typical unchannelized basin is to increase the contributing area per unit length by several-fold, perhaps typically about five times for steep basins. The magnitude of the increase is inversely proportional to the ratio of hollow to basin width because it is assumed that flow lines are perpendicular to surface contours in the hollow. With these limitations in mind we can rewrite (26) to

account for flow convergence:

$$h = \frac{cR_0L}{K_s \sin\theta \cos\theta} \tag{27}$$

The equation shows that for a given rainfall the depth of saturation increases with gentler slopes, larger hydraulic conductivity, smaller hollow widths, and greater hollow lengths, all of which is physically realistic.

Slope stability

The linkage between basin length, strength properties and hillslope hydrology can be achieved by substituting (27) into (20) and solving for cohesionless soils with basin length L:

$$L = \frac{\rho_s Kz}{c\rho_w R_0} \sin^2\theta \left[\frac{1}{\tan\theta} - \frac{1}{\tan\phi'}\right] \tag{28}$$

Because of the assumption used in deriving (28), it is only valid for hydrostatic pore pressures where the water depth h does not exceed the soil depth; hence $(\rho_s - \rho_w)\rho_s^{-1} \tan\phi' < \tan\theta \leq \tan\phi'$. The upper boundary $\tan\phi'$ defines those slopes that would be unstable under dry conditions. As expected, for a given slope and angle of internal friction, the basin length should be greater for soils with high hydraulic conductivity relative to the rainfall rate and for basins with weak convergent topography. Within the range of applicable $\tan\theta$, L at first declines relatively slowly with hollow gradient, but above $0.7 \tan\phi'$, it declines rapidly to zero at $\tan\theta = \tan\phi'$. Humphrey (1982, p. 122) obtained similar results, although for much shorter slope lengths, for a basin he called an "elongate wedge" in which colluvium mantles a bedrock step. Kirkby (1978, p. 359) has also sketched qualitatively a decreasing distance to divide with increasing slope for a hypothetical hillslope.

The role of climate is expressed in the steady rainfall rate R_0 in (28). The soil depth z is of order 0.1 to 1.0 and for typical unchannelized basins with $c \sim 5$ it appears that the ratio K_s/R_0 should be about 10^3. An assumption used in (28) is that the entire basin is contributing runoff, and for a given R_0 the time required for water from the upslope end of a hollow to reach the channel head is the hollow length divided by the horizontal velocity component of subsurface flow V_s. According to (23), $L/V_s = L(K_s \sin\theta \cos\theta)^{-1}$, which is of the order of 10^6 to 10^7 or 10 to 100 days. This implies that the location of the channel head depends on the cumulative rainfall over a long period and the greater the rainfall over this characteristic period, the shorter the unchannelized basin length. Shorter basins imply higher drainage density; thus (28) agrees with observations that drainage density generally increases with greater precipitation in humid areas (see Dunne, 1980; Abrahams, 1984).

In order to compare the functional relation given in (28) to the field data, we have matched the equation with the field observation that a basin of

$\tan\theta = 0.518$ (27.4°) should be about 140 m long. This allows us to treat all the constants in (28) as one, evaluate it under the assumption that $\phi' = 46°$ (Reneau et al., 1984), and use this constant to depict (28) in Figure 17.9 (broken curve). The regression line from Figure 17.4 is shown for values less than 0.5 $\tan\phi'$. At values close to 0.5 $\tan\phi'$, (28) predicts a length–gradient relationship close to the empirical one. The available field data (eight points) do not indicate whether (28) or the empirical line derived mostly from less steep basins provides a better fit. The rapid decline in length with increasing slope shows that hillslopes close to $\theta = \phi'$ are much less stable than hillslopes only a few degrees less steep. This suggests that slopes with θ approaching ϕ' would be rare; and, in fact, the steepest hollow with a colluvial fill (which has recently failed) that we have found in California is 0.75 $\tan\phi'$ (38°), and few occur above 0.7 $\tan\phi'$. In Oregon and Washington, a survey of road-cuts exposing colluvium-mantled hollows yielded only six hollows with thick deposits steeper than 40° in the 47 hollows observed (Dietrich et al., 1982, Fig. 3A). If the structure of (28) is correct it also suggests that drainage density may rapidly increase on steeper hillslopes. This may explain in part why side slopes, which are steeper than the hollows, often support smaller subhollows (Fig. 17.1). As a final comment, (28) indicates that colluvium strength, as controlled by the angle of internal friction ϕ' strongly influences the required basin length. The form of the broken curve in Figure 17.9 remains unaltered, but

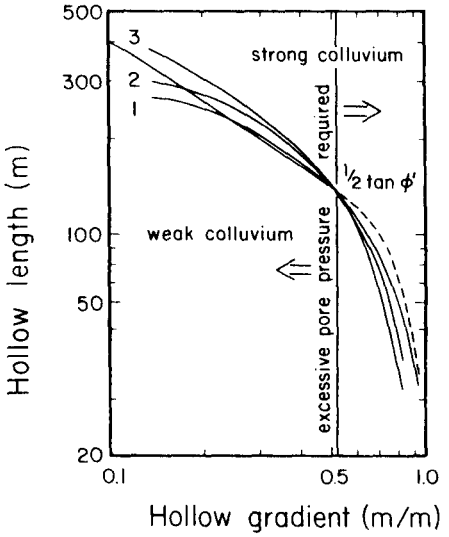

Figure 17.9 Factors controlling the relation of length to hollow gradient in unchannelized basins. The full straight line is the empirical fit to the data. Curves represent results for (29) where $\psi = CL^j(\tan\theta)^k$ and j and k vary with curve number: (1) $j = 1.5$, $k = 0.2$, (2) $j = 1.0$, $k = 0.0$, (3) $j = 1.0$, $k = 0.2$. The broken curve is the calculated relation based on shallow subsurface flow for $\phi' = 46°$.

it is shifted either right or left with corresponding changes in 0.5 tan ϕ'. For example, if $\phi' = 41^\circ$ rather than 46°, at tan $\theta = 0.577$ (30°) the length of the basin would, according to (28), decline by 25 percent, and for steeper slopes the difference in lengths would be much larger.

Groundwater flow

Many of the basins used to define the area, length, and slope relationships presented here have hollow gradients much less than that necessary for instability in the colluvium at saturation. Not only do the high values of angle of internal friction for the coarse textured colluvium suggest this, but saturation overland flow (*sensu* Dunne, 1978) is commonly observed in the downslope ends of the unchannelized basins (e.g., Lehre, 1982; Pierson, 1977; and our own observations in California). Except for the case where a fine-textured soil of low hydraulic conductivity overlies a coarser soil of high conductivity (e.g., Rogers and Selby, 1980) it is probably rare for excessive pore pressures to develop as a result of shallow subsurface flow. High pore pressures and pressure gradients, however, can develop near the surface in the deep groundwater flow system drained at the channel head (Dunne, 1980). These high pore pressures may contribute to the headward advance of a gully at the downslope end of the basin. As in the previous section, then, we propose that the channel head occurs where frequent excessive pore pressure causes erosion of colluvium and prevents burial of the channel. This instability depends both on seepage forces and on the strength of the colluvium. Neglecting the contribution from seepage forces, we can rewrite (20) in terms of pressure head ψ:

$$\psi = \frac{\rho_s z \sin\theta \cos\theta}{\rho_w}\left[\frac{1}{\tan\theta} - \frac{1}{\tan\phi'}\right] \tag{29}$$

Unlike the shallow surface flow, which can be treated as hydrostatic and largely two-dimensional, deeper groundwater flow is not easily approximated algebraically. Intuitively we might expect the pressure head to increase with both slope length and gradient. We have performed a preliminary test of this relationship by numerically modeling flow in a saturated, straight, two-dimensional hillslope using the integrated finite-difference method (Narasimham et al., 1978). Three slope lengths (100, 150, and 200 m) and three gradients (0.125, 0.25 and 0.5) were used. Figure 17.10 shows the equipotential lines (to which the flow is perpendicular) for the 200-m slope of 0.25 gradient, a geometry similar to that observed in the field. The high excessive pore pressures in the lower end of the slope are largely a consequence of the deep downslope vertical boundary on the flow region (lower left wall). This boundary condition is appropriate for the case of the hillslope facing a valley with a slope of comparable size and gradient on the opposite side. For this boundary condition, Figure 17.10B shows the variation in pressure head at 2 m below the surface for a site 5 m upslope from the downslope boundary and

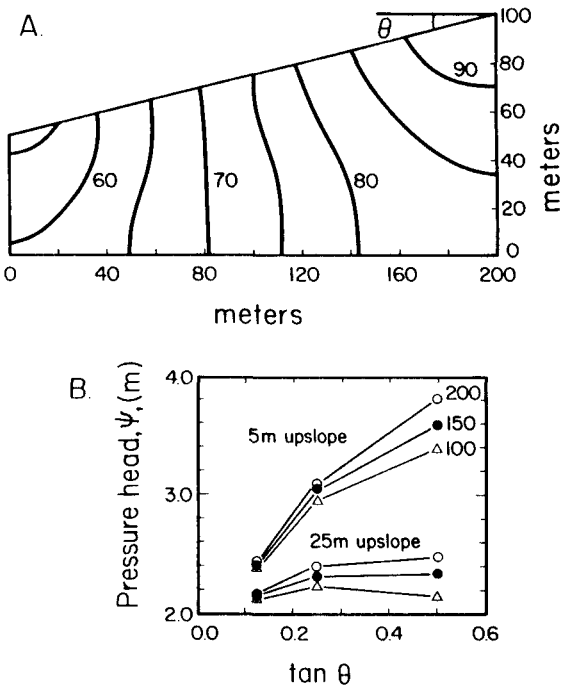

Figure 17.10 Results of numerical modeling: (A) equipotential lines (in meters) in a two-dimensional straight hillslope under complete saturation with a hydraulic conductivity of 10^{-5} cm/s and a surface gradient of 0.25; and (B) changes in pressure head with gradient for slope lengths of 100, 150, and 200 m at two positions 5 m and 25 m upslope.

25 m upslope from the boundary on the three slope lengths and gradients. As anticipated, pressure head ψ varies with both slope length and gradient, with gradient being more important upslope from the boundary. A two orders of magnitude increase in hydraulic conductivity does not significantly alter these pressure values. The actual pressures are strongly dependent on the flow region boundary conditions, but for a variety of geometries the above dependence on slope length and gradient was still observed. Because of the simplification of the natural system represented by the model, it seems unrealistic to attempt to use an equation for ψ as a function of L and $\tan\theta$ that is derived from the numerical model to explain the field relationships. Instead these results primarily suggest that ψ increases with both variables.

Slope stability

Trial and error analysis of substituting values for the exponents in the equation $\psi = CL^j(\tan\theta)^k$, solving for L, and comparing with Figure 17.4 and 17.10 by matching the solution with field data at $0.5 \tan\phi'$ suggests that slope length has a stronger influence than gradient on pressure head (i.e., the exponent j

may be greater than 1.0 and the exponent k less than 0.3). Also, all trials yielded convex-up curves rather than the linear relations fit to the data. L increases very slowly with low values of $\tan\theta$, and at high $\tan\theta$ it increases very rapidly. The predominance of slope length over gradient may be physically correct because L is a surrogate for drainage area, and strong flow convergence towards the seepage face at the channel head may be a major contributor to the requisite pressure head. Further numerical modeling must be done to test this hypothesis.

The trial and error analysis also revealed one other problem. Projection of various solutions for $\tan\theta$ greater than $0.5\tan\phi'$ in all cases gave a curve quite similar to the model based on subsurface flow, but the maximum slope lengths were less. This finding raises the issue of whether shallow subsurface flow or deeper groundwater flow is more important in controlling pore pressures responsible for slope stability. Field observations on pore pressures and flow paths should help solve this problem. Because of the similarity of the results, largely due to the form of

$$\sin\theta\cos\theta\left[\frac{1}{\tan\theta}-\frac{1}{\tan\phi'}\right]$$

in (28) and (29), the conclusions reached in the subsurface flow section regarding drainage density and the angle of internal friction are not altered by this analysis.

An extreme case of "strong" colluvium that under this model would require large excessive pore pressures may occur at the sites studied by Mills (1981) in which massive boulders of quartzite are deposited in relatively low gradient valleys formed in shale. The high angle of internal friction and permeability both prevent the development of instabilities due to high pore pressures and, as Mills proposed, the basins may tend to migrate laterally. In contrast, Hack (1965) presented maps of two hollows in the Martinsburg Shale of Virginia and commented on the fine texture of the hollow colluvium. Based on the position of channel heads shown on the maps, drainage areas were calculated and compared with the regression in Figure 17.4. The areas were 0.63 and 0.72 of those predicted. The fine texture of the colluvium would result in a low angle of internal friction, which should require less drainage area to maintain a channel. The proposed model can be improved by accounting for the seepage forces that undermine channel head walls and, in so doing, bring about slope failure. Although it is possible to write a simple force balance between the weight of the colluvium and the outward-directed drag force caused by seepage (e.g., Dunne, 1980), it is difficult at this point to use it in a model for channel initiation. It is not yet clear whether the channel head tends to be located where the seepage force just equals the weight of the colluvium, or where it exceeds it by some large amount. Also it is difficult to estimate the outward component of the local pressure gradient because it is strongly dependent on the geometry of the flow region. Hopefully future field studies will reveal the most appropriate boundary conditions to use in a model that incorporates seepage forces.

Conclusion

Pieces of a quantitative model for the evolution, geometry, and mechanics of unchannelized basins on soil-mantled hillslopes are beginning to come together. An essential first step is to develop quantitative measures of basin characteristics. Initial field observations suggest that there exists a strong inverse relationship between the drainage area necessary to initiate a channel head and the average hollow gradient of the basin. A similar relationship occurs between hollow length and gradient. These data suggest that steeper slopes should have more exterior link sources, resulting in a greater drainage density. Basin form, consisting of noses, side slopes, and a hollow appears to be well represented by the geometry of a tipped triangular trough and typically the ratio of hollow slope to side slope is about 0.8. Mass balance calculations reveal that rate of thickening of colluvium in the hollow diminishes with time due to increasing cross-sectional area of the hollow, and that basins with steeper side slopes and more convergent topography have high rates of colluvium accumulation.

We have made an initial attempt to explain the field relationships by developing simple approximations for saturation flow depth and pressure head as a function of basin geometry and by using these approximations in the Mohr–Coulomb failure law to predict the hollow length–gradient relationship observed in the field. This analysis has probably raised more questions than it has answered. We have not yet firmly established from quantitative field observation what processes control the position of the channel head at the end of the hollow. Our models suggest that the geometry of low gradient basins is controlled by the development of significant excessive pore pressures and that changes in length and commensurate drainage area are more important than gradient in controlling the pressure head at the downstream sections of basins. Both the subsurface flow and the groundwater flow models, when used in the Mohr–Coulomb failure law, predict for slopes greater than 0.7 $\tan \phi'$ a rapid decline in the slope length necessary to initiate a channel head, consequently, we rarely find basins this steep. Despite the limitations of these many simplistic models, they strongly suggest that area–slope and length–slope relations vary significantly with the strength of the colluvium, particularly the angle of internal friction. They also suggest that the functional relationship for the length–slope curve should be convex-up rather than log-linear. An improvement on the proposed model can be made when seepage forces are properly included.

We have not tackled, by any means, all the major problems concerning unchannelized basin geometry. We do not know what controls the width of these basins. For a given width, it is not yet known what determines either the ratio of hollow slope to side slope or the basin amplitude. Hollow bedrock profiles appear to be concave, but we have insufficient data to attempt generalizations regarding geometry. The cause of the axial concavity is not readily observed either. The mechanism of Calver (1977), whereby bedrock scouring varies in proportion to the frequency of high runoff events which in

turn tend to diminish upslope through the hollow, may be applicable, although in this case the curvature might instead be related to the frequency of landslide-induced exposure of the bedrock surface. In some cases, the concavity may be the result of a curved failure plane within weathered bedrock, as illustrated by Foxx (1984). Finally, as Hack (1965) has emphasized, in many unchannelized basins the principal hollow may have several tributaries or subhollows. These features also dissect the side slopes to major streams. Perhaps, as we have suggested, they arise because the side slopes have steeper gradients than the hollows.

Acknowledgments

J. T. Hack has contributed significantly to this chapter by taking the senior author on a field trip to his study area in Virginia and by freely giving of his ideas and time in several lengthy conversations. H. Mills and C. Hupp also kindly showed the senior author their study areas in Virginia. Valuable conversations were also held with R. Shreve, T. Pierson, N. Humphrey, T. Dunne, C. Wahrhaftig, L. Leopold, M. Power, and R. Dorn. L. Reid helped substantially in analyzing the geometric relationships in a tipped triangular trough. T. Narasimhan gave generously of his time in the development of the integrated finite-difference groundwater flow model. Field observations contributed by W. Trush, K. Whipple, P. Templet, D. Rogers, K. Vincent, J. Sowers, and C. Meade and field assistance given by M. Power, L. Collins, and S. Raugust were essential. L. Leopold, P. Whiting, A. Abrahams, L. Collins, and T. Dunne, made several useful comments on an earlier draft of this manuscript. In response to a telephone conversation, R. Shreve derived the relationship between sources and drainage density. Funding for our research was provided in part by the National Science Foundation (Grant EAR-84-16775).

References

Abrahams, A. D., Channel networks: a geomorphological perspective, *Water Resources Research*, *20*, 161–188, 1984.

Brown, W. R. III, *Overview and summary of a conference on debris flows, landslides and floods in the San Francisco Bay region*, 83 pp., National Academy of Science, Washington D.C., 1984.

Calver, A., Modelling drainage headwater development, *Earth Surface Processes*, *3*, 233–241, 1978.

Carson, M. A., and M. J. Kirkby, *Hillslope Form and Process*, 475 pp., Cambridge University Press, Cambridge, 1972.

Dietrich, W. E., and R. Dorn, Significance of thick deposits of colluvium on hillslopes: a case study involving the use of pollen analysis in the coastal mountains of northern California, *Journal of Geology, 92*, 147–158, 1984.

Dietrich, W. E., T. Dunne, N. F. Humphrey, and L. M. Reid, Construction of sediment budgets for drainage basins, in *Sediment Budgets and Routing in Forested Drainage Basins*, edited by F. J. Swanson, R. J. Janda, T. Dunne, and D. N. Swanston, pp. 5–23, U.S. Department of Agriculture, Forest Service General Technical Report PNW-141, Pacific Northwest Forest and Range Experiment Station, Portland, Oregon, 1982.

Dietrich, W. E., and T. Dunne, Sediment budget for a small catchment in mountainous terrain, *Zeitschrift für Geomorphologie Supplement Band, 29*, 191–206, 1978.

Dunne, T. Field studies of hillslope flow processes, in *Hillslope Hydrology*, edited by M. J. Kirkby, pp. 227–293, Wiley, Chichester, 1978.

Dunne, T., Formation and controls of channel networks, *Progress in Physical Geography, 4*, 211–239, 1980.

Foxx, M., Slope failures in the Felton Quadrangle, 1981–83, and analysis of the factors that control slope failure susceptibility of the Monterey Formation, M.S. thesis, 139 pp., University of California, Santa Cruz, 1984.

Gray, R. E., and G. D. Gardner, Processes of colluvial slope development at McMechen, West Virginia, *Bulletin of the International Association of Engineering Geologists, 16*, 29–32, 1977.

Hack, J. T., Geomorphology of the Shenandoah Valley, Virginia and West Virginia and origin of the residual ore deposits, *U.S. Geological Survey Professional Paper 484*, 1965.

Hack, J. T., and J. C. Goodlett, Geomorphology and forest ecology of a mountain region in the central Appalachians, *U.S. Geological Survey Professional Paper 347*, 1960.

Humphrey, N. F., Pore pressures in debris failure initiation, M.S. thesis, 169 pp., University of Washington, Seattle, 1982.

Iida, T., A hydrological model of estimation of the topographic effect on the saturated throughflow, *Transactions of the Japanese Geomorphological Union, 5*(1), 1–12, 1984.

Iida, T., and K. Okunishi, Development of hillslopes due to landslides, *Zeitschrift für Geomorphologie Supplement Band, 46*, 67–77, 1983.

Keefer, D. K., and A. Johnson, Earth flow morphology, mobilization, and movement, *U.S. Geological Survey Professional Paper 1264*, 1983.

Kirkby, M. J., Hillslope process–response models based on the continuity equation, *Institute of British Geographers Special Publication 3*, 15–30, 1971.

Kirkby, M. J., Implications for sediment transport, in *Hillslope Hydrology*, edited by M. J. Kirkby, pp. 325–363, Wiley, Chichester, 1978.

Kramer, J., Non-seismic liquefaction in fine grained sand, Ph.D. thesis, University of California, Berkeley, 1985.

Lehre, A. K., Sediment mobilization and production from a small mountain catchment: Lone Tree Creek, Marin County, California, Ph.D. thesis, 375 pp., University of California, Berkeley, 1982.

Marcus, A., First-order drainage basin morphology–definition and distribution, *Earth Surface Processes, 5*, 389–398, 1980.

Marron, D. C., Hillslope evolution and the genesis of colluvium in Redwood National Park, northwestern California: the use of soil development in their analysis, Ph.D. thesis, 187 pp., University of California, Berkeley, 1982.

Mills, H. H., Boulder deposits and the retreat of mountain slopes, or "gully gravure" revisited, *Journal of Geology, 89*, 649–660, 1981.

Narasimhan, T. N., T. A. Witherspoon, and A. L. Edwards, Numerical model for saturated-unsaturated flow in deformable porous media, II: the algorithm, *Water Resources Research, 14*, 255–261, 1978.

Pierson, T. C., Factors controlling debris-flow initiation on forested hillslopes in the Oregon Coast Range, Ph.D. thesis, 166 pp., University of Washington, Seattle, 1977.

Reneau, S. L., W. E. Dietrich, C. J. Wilson, and J. D. Rogers, Colluvial deposits and associated landslides in the northern San Francisco Bay area, California, USA, *Proceedings of the 4th International Symposium on Landslides*, pp. 425–430, 1984.

Rogers, J. W., and M. J. Selby, Mechanisms of shallow translational landsliding during summer rainstorms: North Island, New Zealand, *Geografiska Annaler, 62A*, 11–21, 1980.

Shimokawa, E., A natural recovery process of vegetation on landslide scars and landslide periodicity in forested drainage basins, paper presented at the *Symposium on the Effects on Forest Land Use on Erosion and Slope Stability*, Honolulu, Hawaii, May, 1984.

Smith, T. R., and F. P. Bretherton, Stability and conservation of mass in drainage basin evolution, *Water Resources Research, 8*, 1506–1529, 1972.

Swanson, F. J., R. L. Fredricksen, and F. M. McCorison, Material transfer in a western Oregon forested watershed, in *Analysis of Coniferous Forest Ecosystems*, edited by R. L. Edmonds, pp. 233–266, Dowden, Hutchinson, and Ross, Stroudsburg, Pa., 1982.

Swanston, D. N., and F. J. Swanson, Timber harvesting, mass erosion, and steepland forest geomorphology in the Pacific Northwest, in *Geomorphology and Engineering*, edited by D. R. Coates, pp. 199–221, Dowden, Hutchinson, and Ross, Stroudsburg, Pa., 1976.

Tanaka, T., The role of subsurface water exfiltration in soil erosion processes, *International Association of Hydrological Scientists Publication, 137*, 73–80, 1982.

Tsukamoto, Y., and O. Kusakobe, Vegetative influences on debris slide occurrences on steep slopes in Japan. Paper presented at the *Symposium on the Effects of Forest Land Use on Erosion and Slope Stability*, Honolulu, Hawaii, May, 1984.

Tsukamoto, Y., T. Ohat, and H. Noguchi, Hydrological and geomorphological studies of debris slides on forested hillslopes in Japan, *International Association of Hydrological Scientists Publication, 137*, 89–98, 1982.

Woodruff, J. F., Debris avalanche as an erosional agent in the Appalachian Mountains, *Journal of Geography, 70*, 399–406, 1971.